Lewis Acid Passivation of Mechanically Exfoliated Black Phosphorus

Yukako Sakazaki

A thesis

submitted in partial fulfillment of the

requirements for the degree of

Master of Science

University of Washington

2019

Committee:

Alexandra Velian

Robert Synovec

Program Authorized to Offer Degree:

Chemistry

University of Washington

Abstract

Lewis Acid Passivation of Mechanically Exfoliated Black Phosphorus

Yukako Sakazaki

Chair of the Supervisory Committee:
Assistant Professor Alexandra Velian
Department of Chemistry

Exfoliated black phosphorus (*exf*-BP) is a 2D material with a tunable bandgap and favorable electron transport properties for optoelectronic applications. However, its instability under ambient conditions presents challenges for successful integration into devices. Here, we present a chemical treatment method as a convenient, effective strategy for passivation. We treat the *exf*-BP flakes with Lewis acids (gallanes, alanes, boranes), many of which interact with and stabilize the *exf*-BP surface against ambient degradation. Ambient stability is tracked with a combination of optical microscopy (OM) and atomic force microscopy (AFM). Both methods reveal that Lewis acid-treated *exf*-BP flakes have enhanced ambient stability. Moreover, the effectivity of the stabilization increases with the calculated bond dissociation energy (BDE) of adducts formed between the Lewis acid and molecular phosphine analogues. $AlBr_3$, which was

found to be the most effective of the Lewis acids tested, was used to fabricate a passivated *exf*-BP field-effect transistor (FET). The $AlBr_3$-treated *exf*-BP FET shows similar gate modulation, *I*–*V*, photocurrent, and stability as a typical AlO_x-encapsulated *exf*-BP FET. Thus, the $AlBr_3$ treatment method may serve as a useful alternative to AlO_x passivation *via* atomic layer deposition (ALD).

TABLE OF CONTENTS

LIST OF FIGURES

ACKNOWLEDGEMENTS

Firstly, I would like to express my gratitude to my advisor, Prof. Alexandra Velian, for her continuous support and mentorship throughout this graduate school experience. She has taught me so much about the practice of science, and I am tremendously grateful for her training, guidance, and words of encouragement.

I would also like to thank all the members in the Velian group: [2D subgroup] Christine Chang, Dr. Daniel Tofan, Kendahl Walz, David Hales, Akshit Patel, [Clusters subgroup] Jonathan Kephart, Benjamin Mitchell, and Dr. Andrei Chirila, as well as former members: Andrew Boggiano, Muammer Yaman, Elizabeth Ramirez, Luke Chang, Hao Yin, and Alex Bard. I am so grateful to these "Velian's Villains" for not only creating an exciting and supportive lab environment to work in, but also providing invaluable advice for carrying out my research.

I would also like to thank all the groups in the Inorganic Chemistry Division: Goldberg group, Heinekey group, Cossairt group, Kovacs group, Gamelin group, Michael group, and the Lalic group. I am thankful for the kind help and support I received from the members of these groups, as well as their well-decorated hallways and office spaces. I would like to thank Dr. Kelly Kim, who was a wonderful mentor during undergraduate research at Caltech and continued to support and encourage me at UW. I would like to thank the Chemistry Department for providing a safe, healthy, and friendly workplace.

I am also grateful for my collaborators in the Electrical Engineering Department: Ruoming Peng and Seokhyeong Lee in the Mo Li group, as well as the Materials Research Science and

Engineering Center (MRSEC) at UW, which instituted the collaboration. I would also like to thank collaborators in the Physics Department, Chenfeng Du in the Xiaodong Xu group for the training and advice on the use of optical microscopy, along with William Holden in the Seidler group for phosphorus X-ray Emission Spectroscopy (XES).

Part of this work was conducted at the Molecular Analysis Facility, a National Nanotechnology Coordinated Infrastructure site at the University of Washington which is supported in part by the National Science Foundation (grant ECC-1542101), the University of Washington, the Molecular Engineering & Sciences Institute, the Clean Energy Institute, and the National Institutes of Health. I am especially grateful for Dr. Micah Glaz, who trained me on the Atomic Force Microscope (AFM) and spent countless hours troubleshooting the instrument.

Finally, I am grateful to my parents, sister, husband, friends, and church community for all their support, inspiration, and love. Thank you all so much!

Section 1: Introduction

Black phosphorus (BP) is the most thermodynamically stable allotrope of phosphorus (P).[1] It is a van der Waals layered material with an orthorhombic crystal structure.[2] Individual sheets are puckered and contain P_6 rings in chair conformations.[3,4] Each P atom is sp^3-hybridized and bound covalently to three other P atoms.

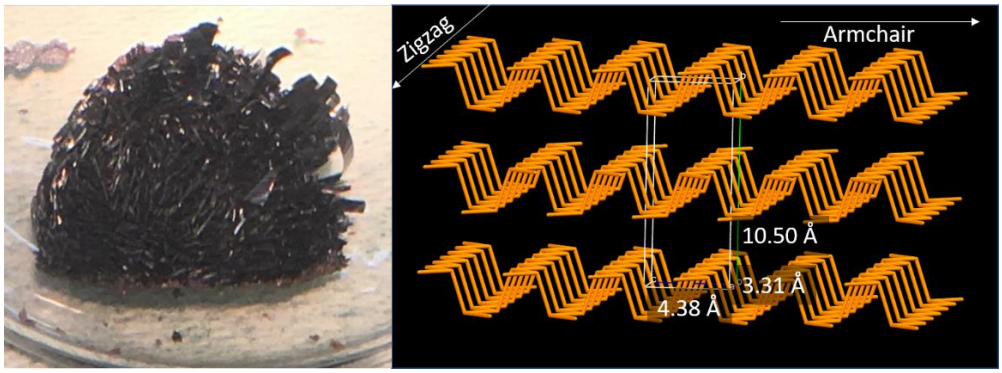

Figure 1.1. Bulk BP crystal (left)[5] and its crystal structure (right).

BP was first synthesized in 1914 by Bridgman *via* treatment of white phosphorus at 200 ºC and 1.2 GPa for 30 minutes.[6] The most recent method of preparing high quality BP crystals at scale was developed by Nilges in 2014.[7] This solid-state synthesis involves the vapor transport growth of BP crystals by high-temperature treatment (gradual cooling from 650 ºC to 550 ºC over 7.5 hours) of red phosphorus, in a quartz ampule using Sn and SnI_4 as mineralization additives. Although BP commercially remains scarcely available and costs *ca*. $560/g, the development of this method has facilitated the dramatic increase in black phosphorus research over the recent years.

1.1 Black Phosphorus as a 2D Material

2D black phosphorus was first prepared by Ye and co-workers in 2014 via micromechanical cleavage of a BP crystal followed by transfer onto a SiO_2/Si substrate.[8] This process, also known as "mechanical exfoliation" or the "Scotch tape method," has been used to prepare many other 2D materials including graphene and 2D-MoS_2.[9,10]

2D black phosphorus has unique properties that are desirable for many device applications. For example, it is a semiconductor with a layer-dependent, intrinsic direct bandgap that changes from 0.3 eV in bulk to 2.3 eV in monolayer BP (Figure 1.2).[8,11] The wide bandgap tunability allows BP to be used in a variety of applications spanning from the visible to mid-infrared spectral range. Multilayer BP is especially useful for mid-infrared photodetection, which would be challenging with other 2D materials due to bandgap limitations.[12] 2D black phosphorus also has a high carrier mobility (1000 $cm^2V^{-1}s^{-1}$) at room temperature[8] as well as a high current on/off ratio,[13] which are important for battery and transistor applications. Finally, due to its unusual structure featuring "zigzag" and "armchair" directions in each 2D plane, BP has highly anisotropic optical and transport properties, which are useful for electronic, optoelectronic, and thermoelectric applications.[14]

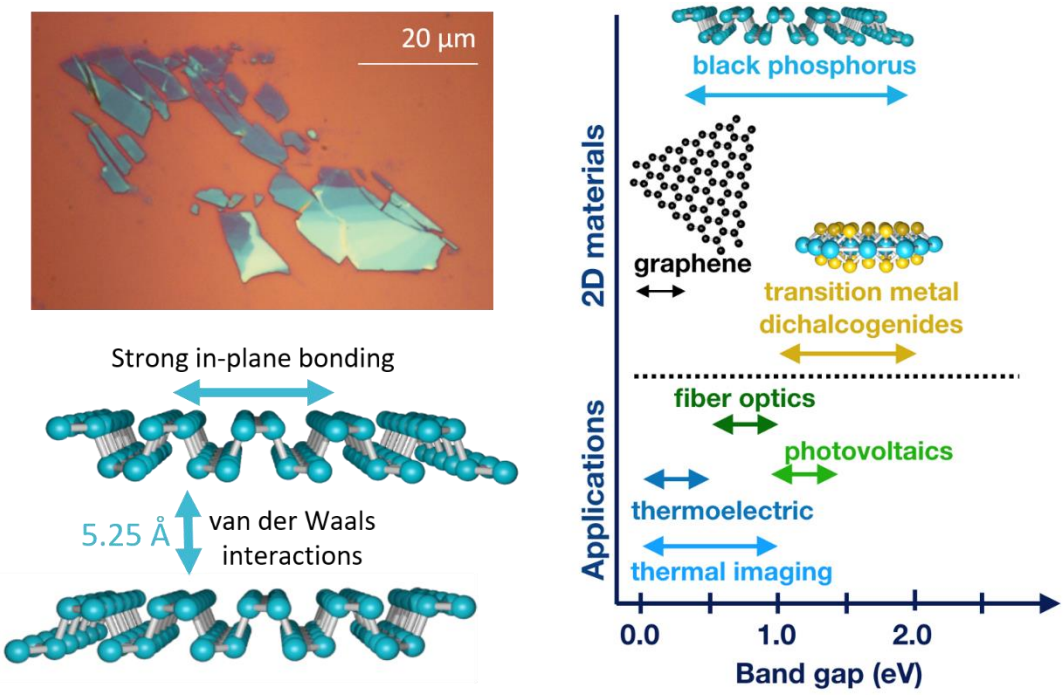

Figure 1.2. Optical microscope image of mechanically exfoliated BP (top left), a structure of bilayer BP showing inter- and in-plane interactions (bottom left),[15] layer-dependent bandgap of BP compared to other 2D materials (right).[16,17]

1.2 Challenges and Existing Solutions

2D black phosphorus has a major Achilles' heel, however, as it degrades under ambient conditions.[18] In a normal lab environment, degradation of freshly exfoliated black phosphorus can be observed within a few hours. The surface of a thin black phosphorus flake first oxidizes to P_xO_y, which further reacts to form phosphoric acid. The phosphoric acid absorbs water and forms small droplets on the surface, which coalesce to form larger droplets as the degradation progresses. The degradation is induced by light, water vapor, and oxygen, as the absence of any of these components slows down the degradation process. Thinner flakes of BP tend to degrade faster than thicker flakes, which is due to quantum confinement effects.[18] Having fewer layers shifts the

bandgap to higher energies, which leads to a stronger overlap between the BP band edge and oxygen acceptors.[17,18]

Most existing methods for passivation can be categorized into chemical functionalization and encapsulation.[19] Chemical functionalization methods involve treating the flakes with chemicals to stabilize the surface against oxidation, while encapsulation methods involve physically protecting the flake with a barrier to keep oxygen and water molecules away from the surface. Chemical functionalization includes covalent and non-covalent methods, where covalent functionalization indicates that the stabilizing molecules are bound to the surface covalently, while non-covalent functionalization indicates that the stabilizing molecules are coordinated or adsorbed onto the surface. Some existing methods of covalently functionalizing 2D black phosphorus include treatment with aryl diazonium salts,[20] iodonium salts,[21] and azides.[22] Some existing methods of non-covalently functionalizing 2D black phosphorus include coordination with titanium sulfonate (TiL_4),[23] 7,7,8,8-tetracyano-*p*-quinodimethane (TCNQ) and perylene diimide,[24] anthraquinone,[25] and ionic liquids.[26] Some encapsulation strategies include passivation with a layer of aluminum oxides (AlO_x) via atomic layer deposition (ALD),[27] as well as coating with other layered materials such as graphene and hexagonal boron nitride (*h*BN).[28]

1.3 Molecular Phosphorus Chemistry with Lewis Acids

Lewis acids are acceptors of electron pairs, as established through extensive research studies by Lewis, Robinson, Ingold and others during 1923-1938.[29] In particular, electron deficient species such as boranes or protons act as Lewis acids, while molecules that contain lone electron pairs, such as phosphines and amines, act as Lewis bases toward these electron deficient species. According to this definition, 2D black phosphorus with its lone pairs on every P atom may act as a Lewis base toward a strong Lewis acid such as boranes (BR_3), gallanes (GaR_3), and alanes

(AlR_3). This Lewis acid-base interaction may be stabilizing, as 2D black phosphorus is vulnerable to oxidation due to its lone pairs and their interaction with oxygen-based species in the atmosphere. Therefore, the interaction of 2D black phosphorus with Lewis acids may protect the material from further degradative oxidation under ambient conditions.

If the Lewis acid-base interaction indeed protects the 2D black phosphorus, we may be able to gain an insight on how strong the interactions between 2D black phosphorus and various Lewis acids are, based on how effectively each Lewis acid protects the 2D black phosphorus. We hypothesize that 2D black phosphorus will follow similar trends as molecular phosphines, due to their similarities in local geometry.

According to density functional theory (DFT) calculations by Gilbert and co-workers,[30] $B(CF_3)_3$ forms a slightly stronger adduct to phosphines than $Al(CF_3)_3$ does (ΔE_{DA} = 70 kcal/mol for $(F_3C)_3BPEt_3$, ΔE_{DA} = 51 kcal/mol for $(F_3C)_3AlPEt_3$), due to the borane being a stronger Lewis acid than the corresponding alane. On the other hand, $B(C_6F_5)_3$ forms a slightly weaker adduct to phosphines than $Al(C_6F_5)_3$, due to steric effects (ΔE_{DA} = 36 kcal/mol for $(F_5C_6)_3BPEt_3$, ΔE_{DA} = 39 kcal/mol for $(F_5C_6)_3AlPEt_3$).[30] The bulky pentafluorophenyl groups are more crowded around the small boron center compared to the aluminum. As bulkier phosphines are used, the systems with $Al(C_6F_5)_3$ do not show any decrease in the dissociation energies (ΔE_{DA} = 42 kcal/mol for $(F_5C_6)_3AlP(t\text{-}Bu)_3$), while for $B(C_6F_5)_3$ systems, the dissociation energy decreases steadily until practically no interaction is seen in $(F_5C_6)_3BP(t\text{-}Bu)_3$ (ΔE_{DA} = 19 kcal/mol). According to theoretical calculations by Timoshkin and co-workers, the strengths of interaction between $M(C_6F_5)_3$ (M = Al, Ga, B) with phosphine is comparable to those of the corresponding trihalides (MCl_3).[31] In the MCl_3 series, the interaction strength with phosphine is found to be greatest with $AlCl_3$ (ΔE_{DA} = 66.4 kJ/mol), followed by $GaCl_3$ (56.7 kJ/mol), and BCl_3 (13.5 kJ/mol).

Section 2: Results and Discussion

2.1 Characterization of Mechanically Exfoliated Black Phosphorus (*exf-BP)*

First, the black phosphorus was exfoliated using the micromechanical cleavage and subsequent transfer to silicon substrates, and they have been characterized by a few different methods to ensure the integrity of the material and serve as a point of comparison for experiments.

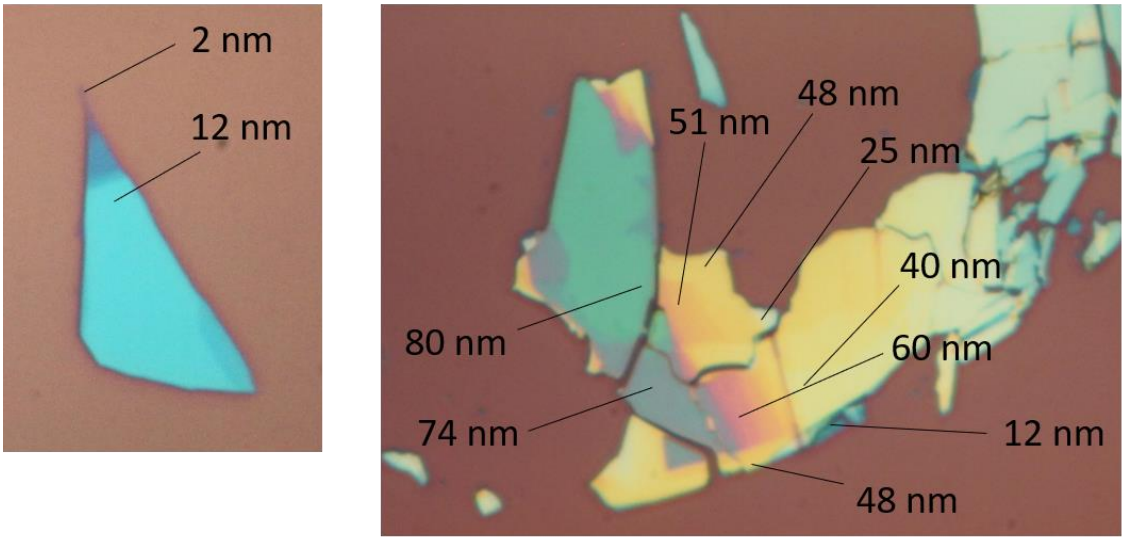

Figure 2.1. Optical microscope (OM) images of *exf*-BP with thicknesses estimated from atomic force microscopy (AFM) in Figure 2.2.

2D materials with a layer-dependent bandgap often show varying colors, or optical contrasts, which have been used extensively to determine thicknesses of 2D materials.[32] Especially for a 2D material like black phosphorus which has a wide range of thickness dependence on the bandgap, flakes of varying thicknesses deposited on a silicon wafer would appear in a multitude of colors.[33] In order to gain an approximate idea of how the colors and opacity correspond to the thicknesses

of the flakes, the optical microscope images of the flakes have been taken, and compared with the heights obtained by atomic force microscopy (AFM). Optical microscope (OM) images of the mechanically exfoliated black phosphorus (exf-BP) were taken immediately after exfoliation in ambient conditions (Figure 2.1). The indicated thicknesses were determined using Atomic Force Microscopy (AFM), as shown in Figure 2.2. The flake to the left has a bright blue color, which indicates thin flakes (< 20 nm thick), whereas white, yellow, orange, pink, lavender, and turquoise colors indicate thicker flakes.

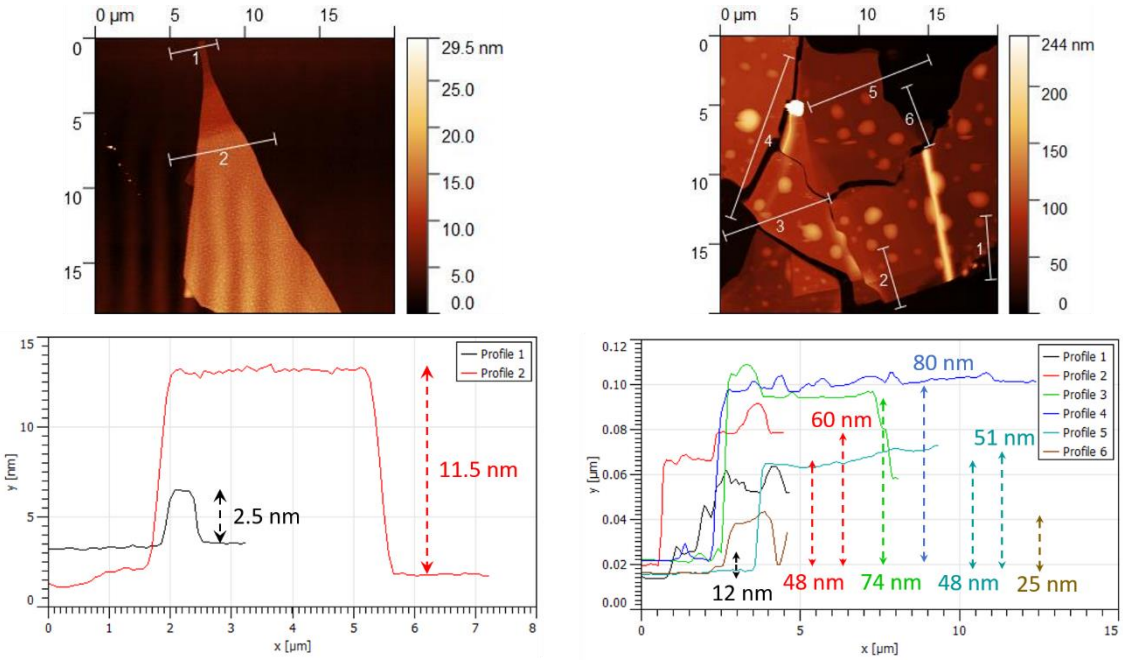

Figure 2.2. Atomic Force Microscope (AFM) images of *exf*-BP obtained for height profile calculations.

After storage in glovebox for 3 days following the initial optical microscopy imaging, the AFM images of the same *exf*-BP flakes shown in Figure 2.1 were obtained and their heights at various locations of the flakes were determined (Figure 2.2). However, oxidation of the top several

layers may introduce error to the measurement, so the heights are approximate. (Note: Local height variation due to oxidation bubbles was not included in approximating the flake thickness.)

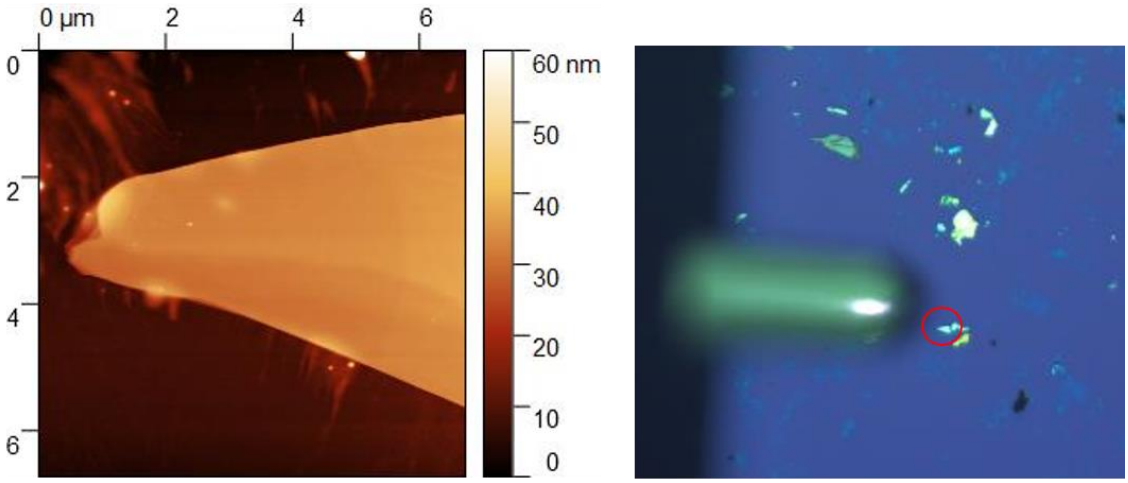

Figure 2.3. Atomic Force Microscope (AFM) images of pristine *exf*-BP before ambient exposure.

To confirm the integrity of our pristine mechanically exfoliated BP (*exf*-BP) flakes before any exposure to ambient exposure, Atomic Force Microscope (AFM) images were taken (Figure 2.3). The smooth surface indicates that the oxidation bubbles from degradation to phosphoric acid has not formed yet. Thus, we may trust the glovebox atmosphere to keep the 2D BP from degrading for a few days.

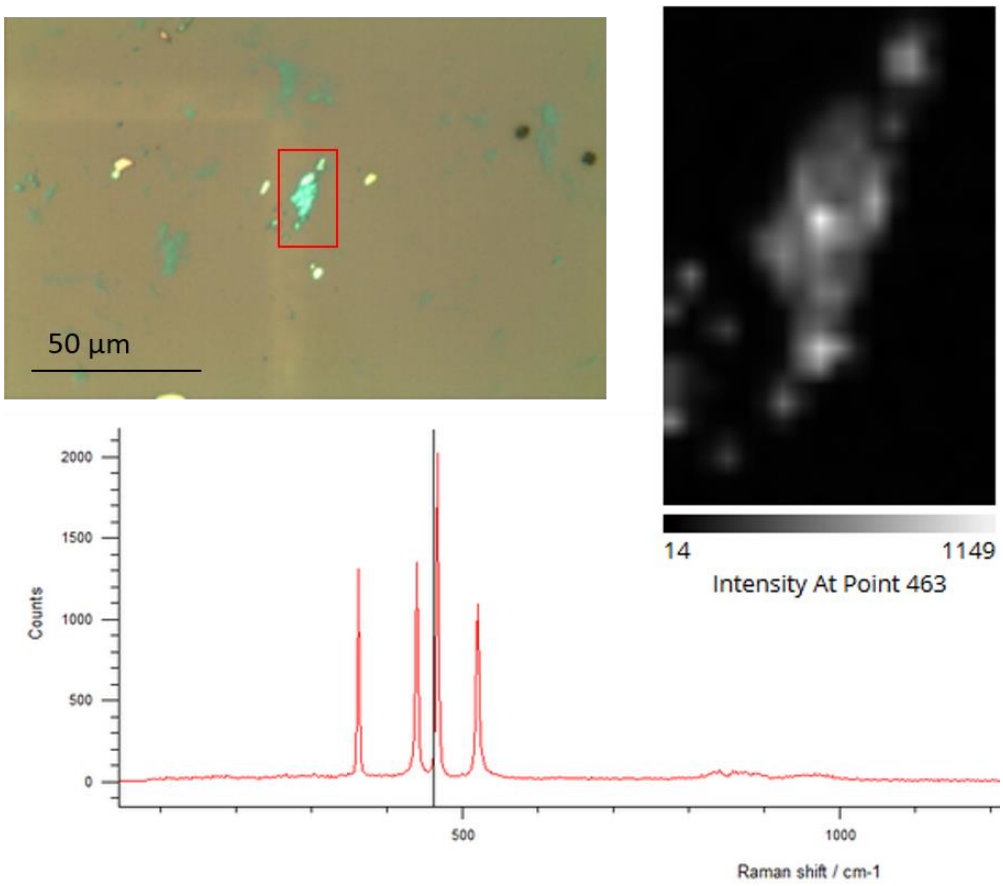

Figure 2.4. Raman spectrum of pristine *exf*-BP (bottom) with a microscope image (top left) and an intensity mapping at 463 cm^{-1} (top right).

To further support successful exfoliation of the black phosphorus, Raman spectra of pristine mechanically exfoliated black phosphorus (*exf*-BP) were taken (Figure 2.4, bottom). A flake of desirable thickness (~20 nm) was identified under the optical microscope (Figure 2.4, top left). Relatively thin flakes were chosen for Raman, as to maximize the representation of any surface functionalization effects for Lewis acid-treated flakes in the spectra. The thinner flakes tend to be a bright turquoise color under the Raman instrument optical microscope. The flake region corresponds well to the Raman intensity mapping (Figure 2.4, top left) at 463 cm^{-1}, which is near the A_g^2 mode, the strongest of the three characteristic black phosphorus signals (A_g^1, B_{2g}, and A_g^2) in the Raman spectra shown.[18] The mapping helps visualize the overlap between the Raman

intensity at this frequency and the flake region visible in the optical microscope, confirming that the flake is indeed black phosphorus.

2.2 Characterization of Lewis Acid-treated *exf*-BP

Next, we treated *exf*-BP flakes with a variety of commercially available Lewis acids with differing strengths: gallium chloride ($GaCl_3$), aluminum bromide ($AlBr_3$), aluminum chloride ($AlCl_3$), aluminum tri-*sec*-butoxide ($Al(O^sBu)_3$), aluminum stearate ($Al(O_2CC_{17}H_{35})_3$), tris(pentafluorophenyl)borane ($B(C_6F_5)_3$), triphenylborane (BPh_3), and boron tribromide (BBr_3).

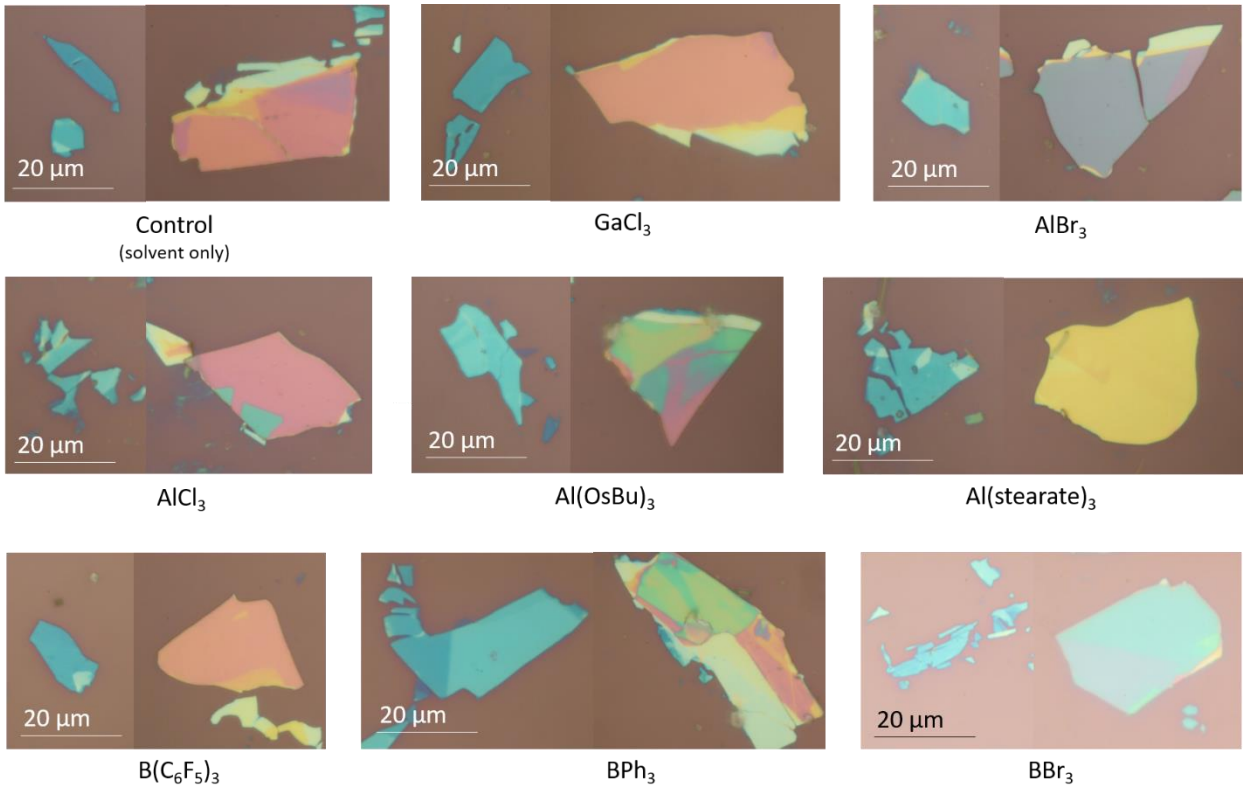

Figure 2.5. Optical microscope images of Lewis Acid-treated *exf*-BP. For each sample represented are a thin flake (left side) and a thick flake (right side), displayed at the same magnification.

First, optical microscope images of mechanically exfoliated black phosphorus (*exf*-BP) treated with Lewis acids were taken (Figure 2.5). To discount any solvent effects, a control sample which has been exposed to the solvents used in the Lewis acid treatment and washing has also been included. In Figure 2.5, two flakes for each sample are represented, one thin (left, < 20 nm thickness) and one thick (right, > 20 nm). Flakes for each sample do not show any variable signs of degradation, such as bubble formation.

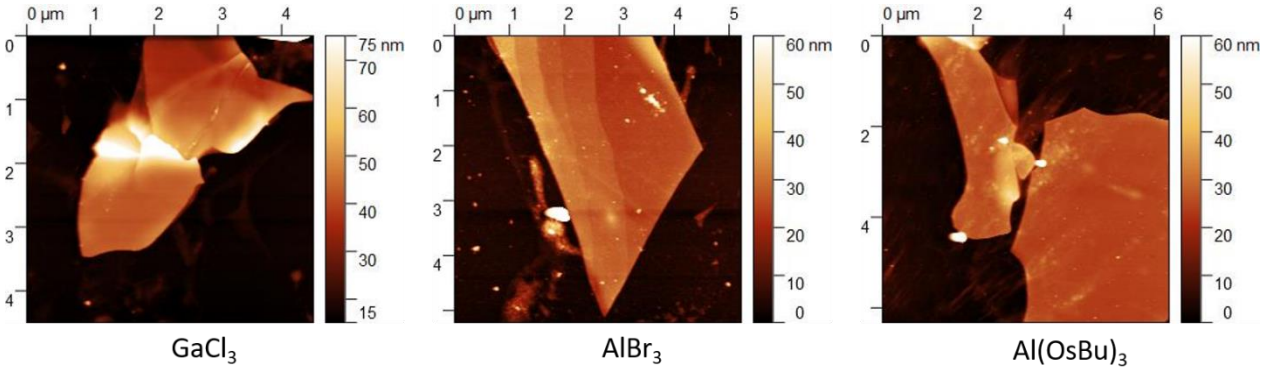

Figure 2.6. Atomic force microscope (AFM) images of Lewis Acid-treated *exf*-BP.

Next, Atomic force microscopy (AFM) images of *exf*-BP treated with the Lewis acids $GaCl_3$ (left), $AlBr_3$ (middle), and $Al(O^sBu)_3$ (right) were taken (Figure 2.6). All three flakes appear to be smooth like the control sample. The flakes look intact with no noticeable bubble formation, indicating that the Lewis acid treatment does not degrade the *exf*-BP.

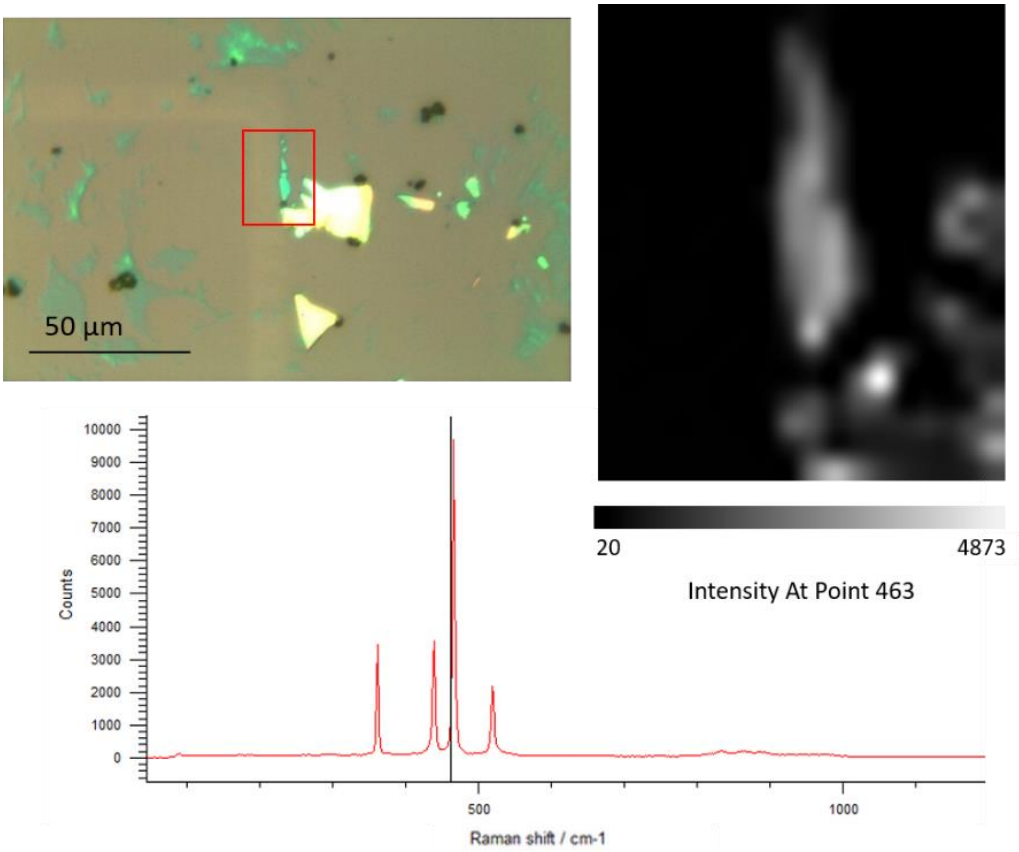

Figure 2.7. Raman microscope spectra (bottom), image (top left), and intensity mapping (top right) of $GaCl_3$-treated *exf*-BP.

To further confirm that the Lewis acid treatment does not degrade the *exf*-BP and preserves its lattice, we took Raman spectra of *exf*-BP treated with a few of the Lewis acids, such as $AlBr_3$, $GaCl_3$, and BPh_3. Figure 2.7 shows the Raman spectra and intensity mapping of *exf*-BP treated with $GaCl_3$. For all three Lewis acids measured (Figure 2.7, Figure A1, Figure A2), a correlation between the intensity mapping at 463 cm^{-1} and the flake region was visible, and all spectra on the flake showed the characteristic black phosphorus signals. Thus, the Lewis acid treatment does not disrupt the crystal structure of the *exf*-BP or cause degradation. No obvious new features are observed using Raman.

2.3 Ambient Stability Test of Lewis Acid-treated *exf*-BP

Once the Lewis acid-treated *exf*-BP has been characterized, we exposed them to ambient conditions to determine whether the Lewis acid treatment stabilizes the *exf*-BP against ambient degradation. The Lewis acids $GaCl_3$, $AlBr_3$, $AlCl_3$, $Al(O^sBu)_3$, $Al(O_2CC_{17}H_{35})_3$, $B(C_6F_5)_3$, BPh_3, and BBr_3 were tested for stabilization of *exf*-BP.

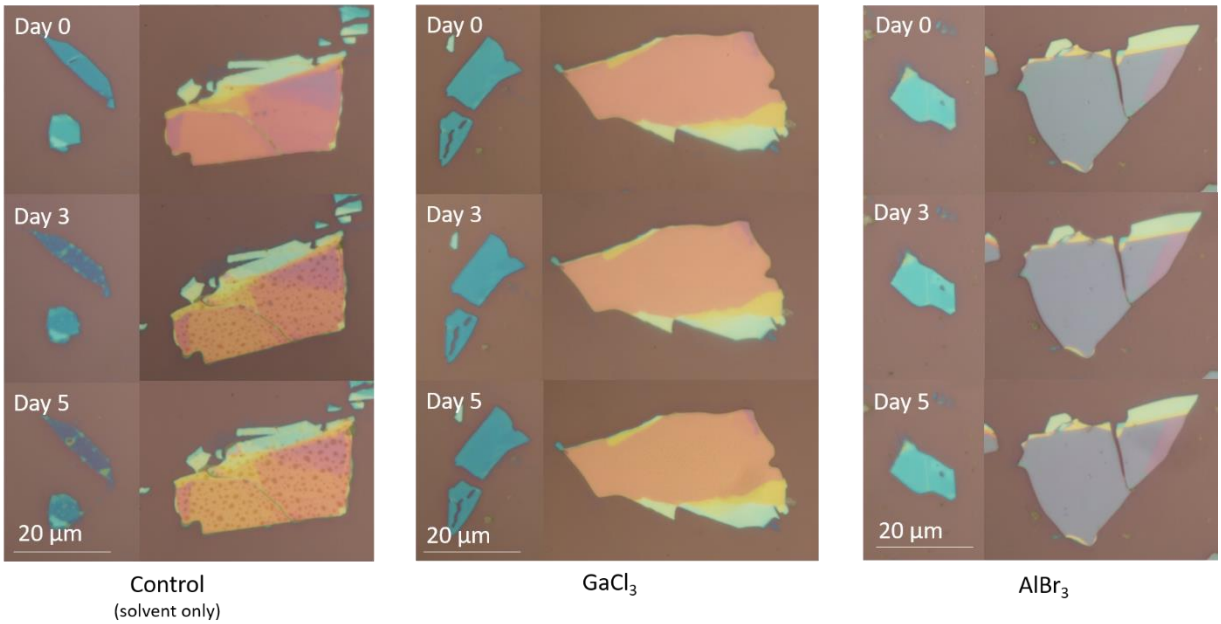

Figure 2.8. Optical Microscope (OM) ambient stability test of *exf*-BP treated with $GaCl_3$ and $AlBr_3$, compared with the control.

We first tested the ambient stability of Lewis acid-treated *exf*-BP by taking optical microscope (OM) images of the same flakes over several days. We were pleased to find that according to OM, $GaCl_3$ and $AlBr_3$ are effective at stabilizing the *exf*-BP against ambient degradation. Figure 2.8 shows the appearance of *exf*-BP treated with $GaCl_3$ and $AlBr_3$ over 5 days, imaged with OM. The control sample, which has been exposed to the same solvents as the treated samples, show significant signs of degradation, including the fading blue color in the thinner flake and bubble formation in the thicker flake. On the other hand, the $GaCl_3$ and $AlBr_3$ flakes seem to stay intact

during the same time period, suggesting that these Lewis acids are successfully protecting the black phosphorus flakes.

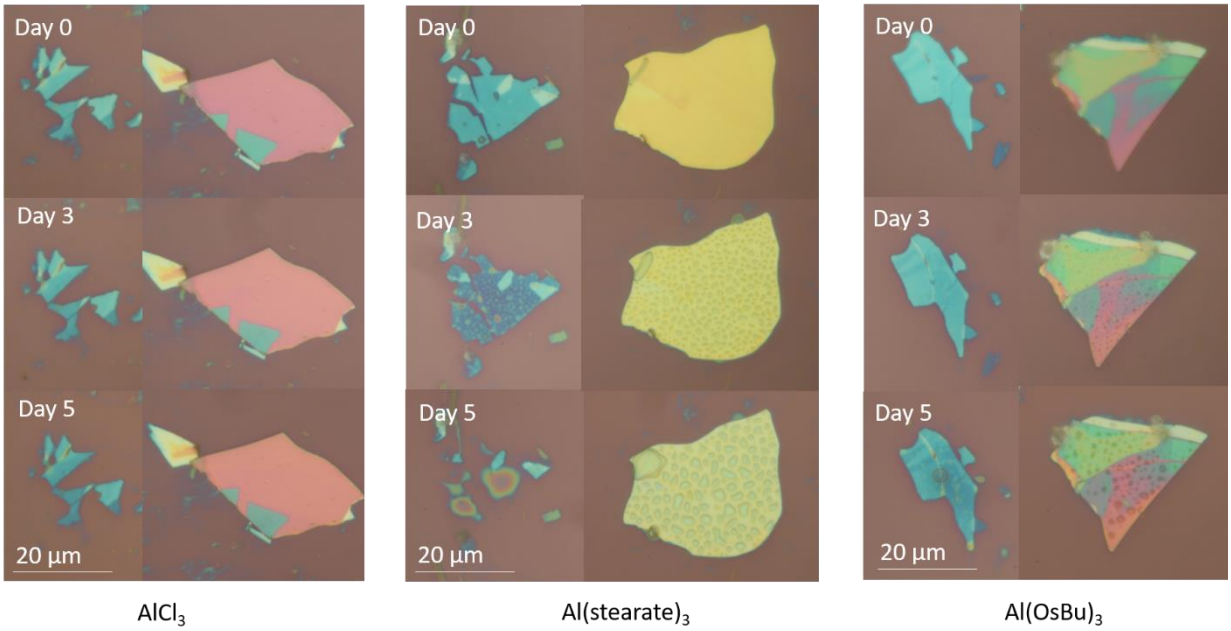

Figure 2.9. Optical Microscope (OM) ambient stability test of *exf*-BP treated with other Al-based Lewis acids. For each sample represented are a thin flake (left side) and a thick flake (right side), displayed at the same magnification.

We continued testing the ambient stability of *exf*-BP samples treated with other Al-based Lewis acids: aluminum chloride ($AlCl_3$), aluminum stearate ($Al(O_2CC_{17}H_{35})_3$), and aluminum *sec*-butoxide ($Al(O^sBu)_3$) using optical microscopy (Figure 2.9). Despite its poor solubility in toluene, aluminum chloride offers significant protection against oxidation. $Al(O_2CC_{17}H_{35})_3$ and $Al(O^sBu)_3$, however, did not offer much protection against ambient degradation of phosphorene. This is most likely due to decreased Lewis acidity with electron-rich groups attached to the aluminum. In particular, the aluminum stearate sample seems to decompose even faster than the control sample. The bubbles of phosphoric acid grow more rapidly on the thick flake, and most of the thin flake

disappears by day 5. We attribute the degradation of the BP flake treated with $Al(O^sBu)_3$ to the weak Lewis acid-base interaction.

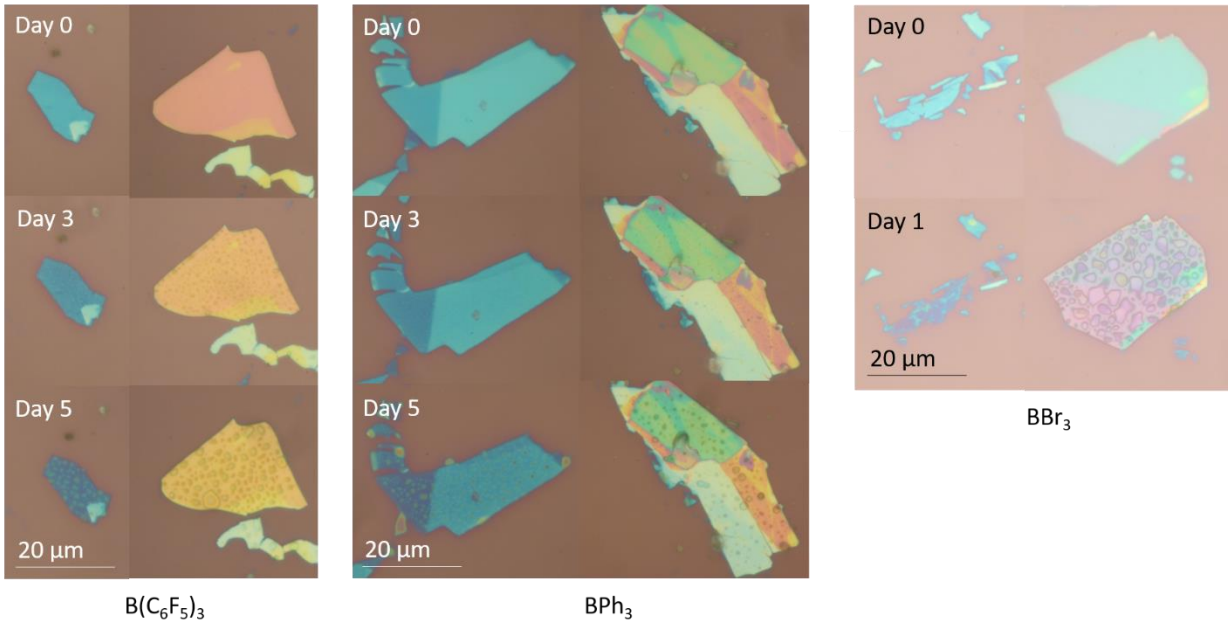

Figure 2.10. Optical Microscope (OM) ambient stability test of B-based Lewis acid-treated *exf*-BP.

We continued with testing the boron-based Lewis acids, tris(pentafluorophenyl)borane ($B(C_6F_5)_3$), triphenylborane (BPh_3), and tribromoborane (BBr_3) using optical microscopy (Figure 2.10). In contrast to the alanes and gallanes, which proved effective, the boranes tested do not offer as much protection against ambient degradation to the *exf*-BP. We first attributed the decreased effectivities of $B(C_6F_5)_3$ and BPh_3 to their added steric bulk, as predicted.[30] We then tested the ambient stability of *exf*-BP treated with BBr_3, which is a very strong Lewis acid, relatively sterically unhindered, and has no solubility problems as it is a liquid. The BBr_3 does not protect the *exf*-BP at all, in fact, it shows even more rapid degradation than the control, forming large bubbles within one day. Thus, we conclude that the poor stability of these borane-treated *exf*-BP

is due to boranes having weaker interactions with phosphines compared to alanes or gallanes in general, as calculated by Timoshkin and co-workers,[31] along with steric and electronic effects from their substituents.

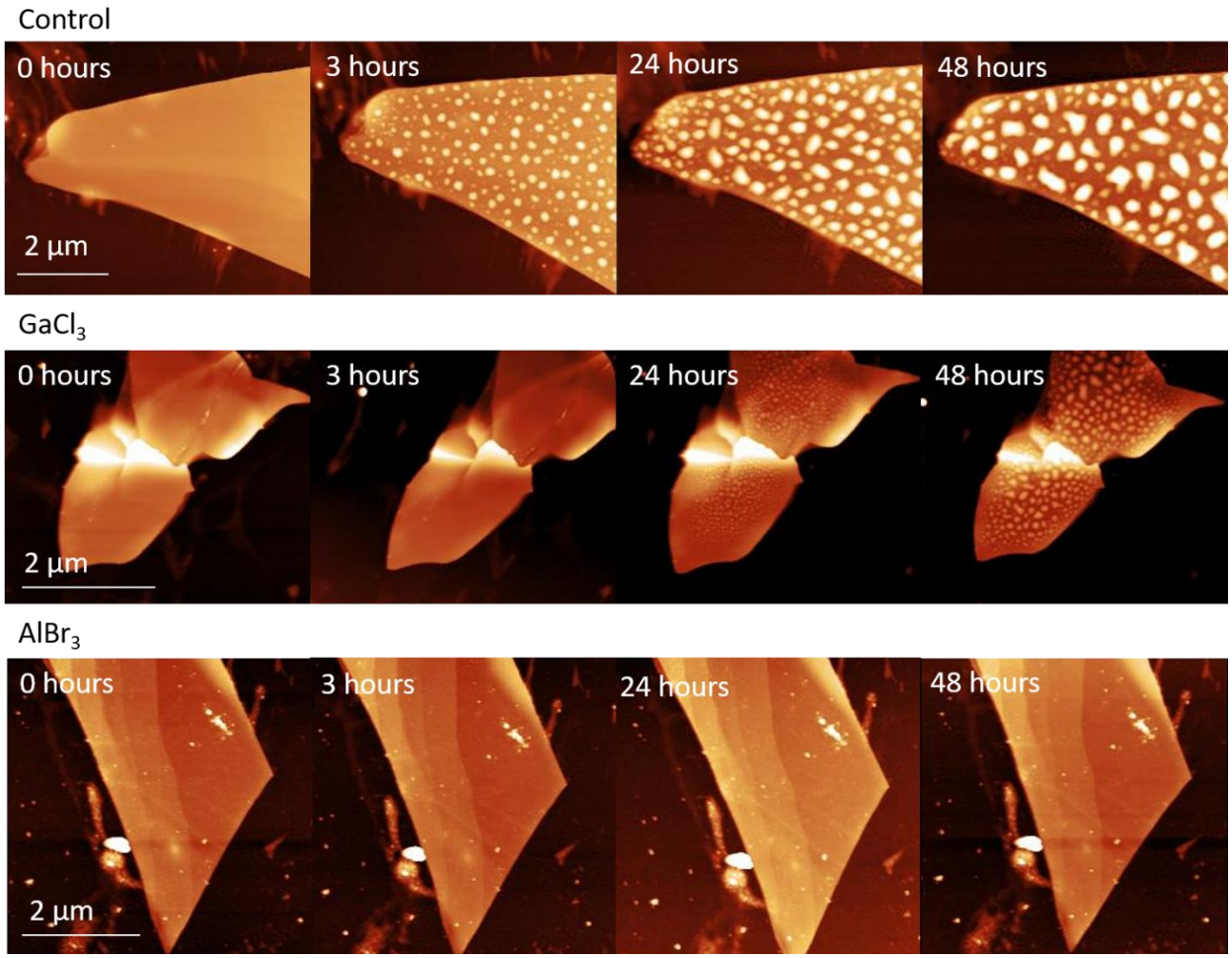

Figure 2.11. Atomic Force Microscopy (AFM) ambient stability test of *exf*-BP treated with selected Lewis acids: gallium trichloride ($GaCl_3$) and aluminum bromide ($AlBr_3$).

Finally, we have tested the ambient stability of *exf*-BP treated with selected Lewis acids, gallium trichloride ($GaCl_3$) and aluminum bromide ($AlBr_3$), using Atomic Force Microscopy, or AFM (Figure 2.11). $GaCl_3$ and $AlBr_3$ were chosen because they provided the best protection for *exf*-BP as seen by optical microscopy and did not present major solubility issues. Since atomic

force microscopy has a higher resolution than optical microscopy, small degradation bubbles which could not be detected in the optical microscopy test of $GaCl_3$ are visible in the AFM stability test starting from ~24 hours after exposure. In contrast, we see no such bubble formation for the $AlBr_3$ sample, even after 4 days (Figure A4). From this observation, we can conclude that $AlBr_3$ treatment of *exf*-BP results in a higher degree of ambient stability than $GaCl_3$. This is most probably due to AlX_3 having a stronger interaction with *exf*-BP than GaX_3 does, which is consistent with the theoretical calculations made in molecular phosphine analogues.[31]

2.4 Device Testing: $AlBr_3$-treated *exf*-BP Field-effect Transistor (FET)

In order to test the effect of Lewis acid-treatment upon the device behavior of the black phosphorus, as well as to test the ambient stability of such devices, $AlBr_3$-treated *exf*-BP field-effect transistors (FET) have been fabricated and tested in collaboration with Ruoming Peng and Seokhyeong Lee in the research group of Mo Li.

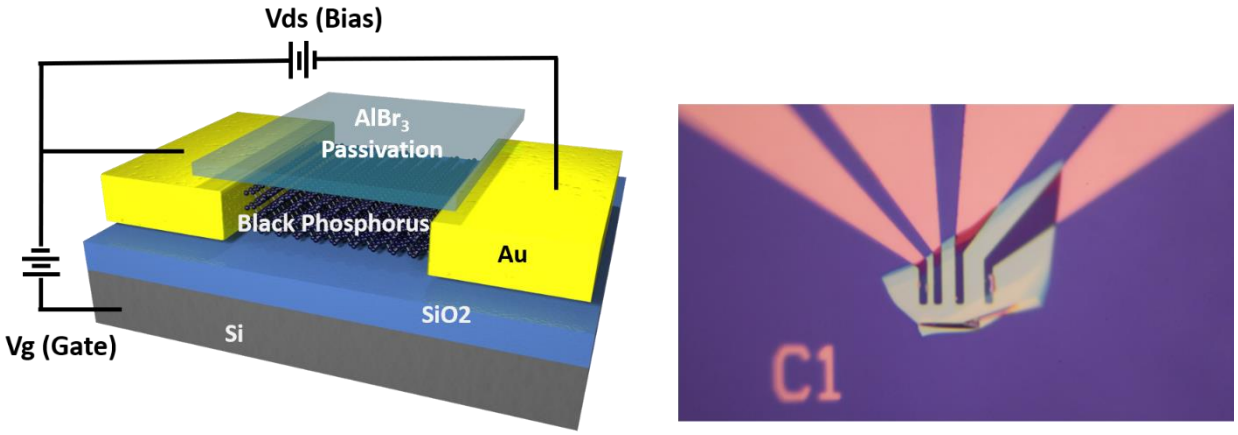

Figure 2.12. Schematic diagram of the $AlBr_3$-treated *exf*-BP FET with back gate (left), and an optical microscope image of the device (right).

The overall structure of the $AlBr_3$-treated *exf*-BP FET is shown in Figure 2.12 (left). An *exf*-BP flake is transferred from a PDMS stamp onto a set of gold electrodes patterned on a 300-nm thermal oxide silicon substrate (Figure 2.12, right). The device is then treated with $AlBr_3$ solution without exposing it to ambient conditions. The device is then exposed to ambient conditions to measure gate modulation, *I*–*V* characteristics, photocurrent, and stability.

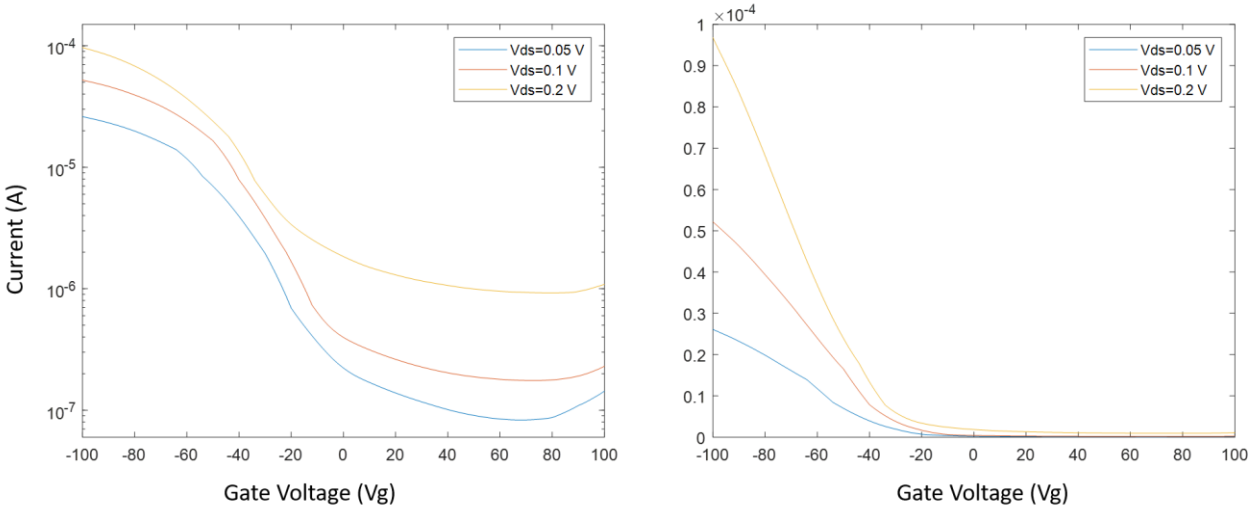

Figure 2.13. Gate modulation behavior of the $AlBr_3$-treated *exf*-BP FET on logarithmic (left) and on normal scale (right).

Figure 2.13 shows the gate modulation behavior of the $AlBr_3$-treated *exf*-BP FET. The current on-off ratio is calculated to be *ca*. 200, which is within the range of previously measured *exf*-BP FETs.[34,35] The device shows good modulation, as the source–drain current can be changed effectively by the gate voltage. The current increases with negative voltages in the Ohmic contact region, while the current decreases with positive voltages in the Schottky contact region. This behavior is comparable to that of a typical *exf*-BP FET that is encapsulated in Al_2O_3 passivation layer *via* atomic layer deposition (ALD).[34]

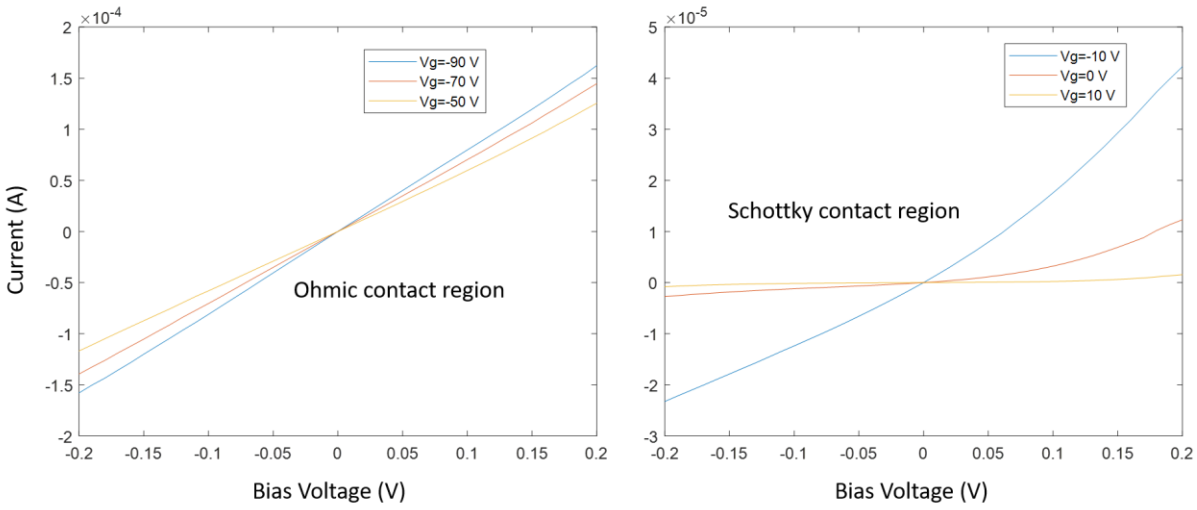

Figure 2.14. *I*–*V* measurements of the $AlBr_3$-treated *exf*-BP FET at different gate voltages, showing Ohmic contact behavior in the high carrier concentration (doping) region (left) and Schottky contact behavior in the low carrier concentration (doping) region (right).

Figure 2.14 shows the *I*–*V* characteristics of the $AlBr_3$-treated *exf*-BP FET at different gate voltages. The voltage to current relationship becomes linear in the Ohmic contact region (negative gate voltages), while the relationship becomes nonlinear in the Schottky contact region (positive gate voltages). This behavior is also comparable to that of a typical *exf*-BP FET encapsulated with Al_2O_3 passivation layer.[34]

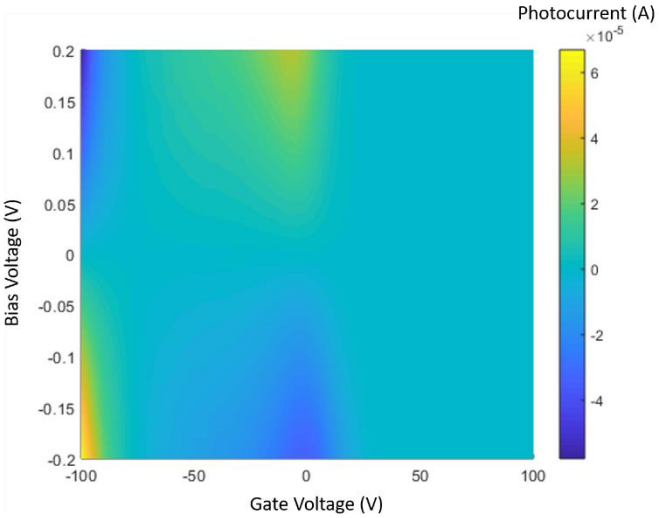

Figure 2.15. Photocurrent mapping results of the $AlBr_3$-treated *exf*-BP FET.

Figure 2.15 shows the photocurrent mapping results of the $AlBr_3$-treated *exf*-BP FET. At gate voltage of 0 V, the photocurrent increases with the bias voltage. This is because the low doping region is dominated by the photovoltaic effect, where the incident light generates electron and hole pairs and causes increase in electric current.[34,36] At gate voltage of -100 V, however, the photocurrent is negative relative to the bias voltage. This is because the high doping region is dominated by the bolometric effect, where the incident light heats the sample and increases phonon scattering, resulting in increased resistance.[34,37] These behaviors also observed in a typical *exf*-BP FET encapsulated in Al_2O_3 passivation layer.[34]

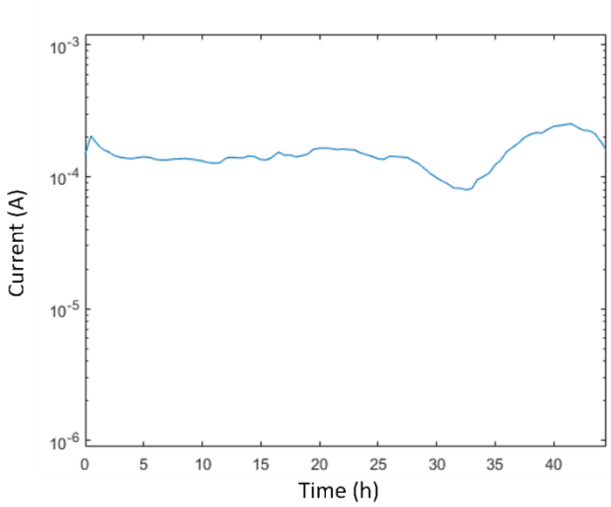

Figure 2.16. Stability calibration of the $AlBr_3$-treated *exf*-BP FET device over the first 45 hours upon ambient exposure.

Figure 2.16 shows the variations in S/D current of the $AlBr_3$-treated *exf*-BP FET over the first 45 hours upon ambient exposure. For *exf*-BP FETs that have not been passivated, the S/D current will decrease by a factor of *ca*. 10^5 over 36 hours.[38] In comparison, the S/D current variations seen thus far in the $AlBr_3$-treated *exf*-BP FET is quite minimal. Clearly, the $AlBr_3$ treatment indeed protects the *exf*-BP from degradation and decrease in device performance.

Section 3: Conclusions

According to optical microscopy (OM), atomic force microscopy (AFM), and Raman, Lewis acids can be used to treat the black phosphorus at the surface, while preserving the underlying black phosphorus structure. Many Lewis acids, such as $AlBr_3$, $GaCl_3$, $AlCl_3$, BPh_3, and $Al(O^sBu)_3$ slowed down the ambient degradation of *exf*-BP to a noticeable degree. From OM, $AlBr_3$, $GaCl_3$, and $AlCl_3$ were found to be most effective at stabilizing the *exf*-BP against ambient degradation. Using AFM, which has higher resolution than OM, $AlBr_3$ was found to be the most effective and

convenient Lewis acid tested, stabilizing the *exf*-BP for at least 4 days without showing signs of bubble formation.

Generally, the ability of a Lewis acid to protect the *exf*-BP against ambient degradation depends on its interaction strength with phosphine, the "molecular analogue" of *exf*-BP. $AlBr_3$ protected the *exf*-BP more effectively than $GaCl_3$, which was much more effective than BBr_3, in accordance with how the central atoms affect the strengths of the Lewis acids' interaction with phosphines. Bulky Lewis acids, such as $B(C_6F_5)_3$ and BPh_3, did not protect the *exf*-BP very well, which is also consistent with how steric factors influence the strength of the Lewis acids' interaction with phosphines. Electronics also played a role, as Lewis acids with electron-rich substituents, such as $Al(O^sBu)_3$ and $Al(O_2CC_{17}H_{35})_3$, were far less effective in protecting the *exf*-BP against ambient degradation.

An $AlBr_3$-treated *exf*-BP FET was fabricated in order to test any changes in the behavior of Lewis acid-treated *exf*-BP devices, as well as stability. From measuring gate modulation, *I–V*, and photocurrent, we may conclude that the $AlBr_3$ treatment does not degrade the optical and electrical properties of typical *exf*-BP FETs encapsulated in Al_2O_3 for stability. More interestingly, current stability measurements show that the $AlBr_3$-treated *exf*-BP FET is stable for at least 45 hours, showing minimal variations in current. Therefore, the $AlBr_3$ treatment imparts stability to the *exf*-BP without changing the behaviors of the pristine black phosphorus to any significant degree. A possibility to be further investigated is that the $AlBr_3$ on the *exf*-BP is oxidized upon ambient exposure to Al_2O_3, forming an atomically thick passivation layer. This may be of considerable utility as an alternative to the conventional Al_2O_3 passivation *via* atomic layer deposition (ALD), as the treatment requires less instrumentation, no exposure to ambient conditions before the passivation, and uses commercially available, reasonably priced chemicals.

Section 4: Experimental

4.1 General Considerations

Unless stated otherwise, all work was performed under an inert atmosphere of N_2 inside of an LC Technology Solutions, Inc. glove box containing <5 ppm H_2O and O_2. Anhydrous solvents were obtained from a SciMatCo solvent system and stored over 3 Å molecular sieves (Thermo-Fisher) for at least 12 h before use; sieves were previously activated by heating at 250 °C under vacuum for at least 3 days. Black phosphorus (BP) crystals (99.998%, Smart Elements) were purchased and used as received. All glassware was dried overnight at 150 °C prior to use. Centrifuge tubes were sealed with O-ring caps to prevent ambient exposure. All plastic items and metal tools, including Scotch tape, vial caps, and tweezers, were evacuated in the glovebox antechamber for at least 12 hours before introduction into the glovebox. Kimwipes and filter papers were dried in the oven at 150 ºC before being brought into the box. When performing mechanical exfoliation in the glovebox, clean nitrile gloves were worn over the glovebox gloves.

All Lewis acids were stored in the glovebox. Aluminum bromide ($AlBr_3$, 99%, Strem) and boron tribromide (BBr_3, *ReagentPlus*, 99.9%, Sigma-Aldrich) were stored in the dark in the glovebox freezer (–35 °C). Gallium(III) chloride ($GaCl_3$, anhydrous, granular, 99.999%-Ga, PURATREM, Strem), tris(pentafluorophenyl)borane ($B(C_6F_5)_3$, min. 97%, Strem), aluminum chloride ($AlCl_3$, anhydrous, reagent, 99%, Strem), aluminum stearate ($Al(O_2CC_{17}H_{35})_3$, Strem), aluminum sec-butoxide ($Al(O^sBu)_3$, Strem), and triphenylborane (BPh_3, min. 95%, Strem), were stored at room temperature in the glovebox. All Lewis acids were used as received from the supplier.

Thermal oxide silicon wafers were purchased from Pure Wafers (285nm SiO_2 Layer on Si (100), single side, 0.5 mm thick, N type P doped, R: 1-10 Ohm-cm), cut to 1 cm x 1 cm size, then

rigorously washed by sequential sonication with Merisuds multi-purpose detergent (diluted ca. 5x in water), deionized water, acetone (HPLC, Fisher), and isopropanol (Certified ACS, Fisher), and then cleaned with a low pressure plasma system (Diener, Femto) immediately prior to use.

Optical microscope (OM) images were acquired on Olympus (BX51M) and Zeiss (Imager.A2m, Axio) microscopes equipped with Canon digital cameras and desktop EOS Utility. Atomic force microscopy (AFM) images were measured in non-contact mode on an Asylum Research Cypher atomic force microscope under a flow of N_2. AFM images were acquired using electrically conductive Cr/Pt AFM probes and processed using the Gwyddion software. Raman spectra were acquired on a Renishaw InVia microscope using a 514 nm Ar laser and a 50× microscope objective.

Mechanically exfoliated black phosphorus flakes, treated or untreated, were imaged or measured directly with OM and AFM on the thermal oxide silicon wafers without further sample preparation steps. Samples were prepared in a glovebox and transported in a container filled with nitrogen until immediately before imaging. To prepare Raman samples, the wafers were sealed to a glass slide in order to prevent oxidation during the Raman measurement, which takes place under ambient conditions.

4.2 Preparation of Starting Materials

4.2.1 *Mechanically Exfoliated Black Phosphorus (*exf-*BP)*

A flat, shiny, small piece (*ca*. 2 mm x 1 mm x 0.1 mm) of black phosphorus crystal (99.998%, Smart Elements) was placed on a piece of Scotch tape (*ca*. 7 cm in length) secured to a clean, flat surface. Another piece of Scotch tape of comparable length was taped over the secured tape and peeled off to cleave the black phosphorus crystal 5-6 times, until thin, slightly iridescent silver crystals are dispersed like a grid onto each piece of Scotch tape. A clean thermal oxide silicon

wafer was secured to the surface, and free exfoliation Scotch tape was gently adhered to the wafer, avoiding trapped bubbles. The tape was peeled off slowly (*ca.* 1 minute per wafer) to maximize flake size and quality.

4.2.2 *Lewis acid solutions*

$GaCl_3$ crystals (26.4 mg, 176.08 g/mol, 0.15 mmol) were dissolved in toluene (3 mL, 2.6 g) in a vial, sealed with Teflon tape and cap, further sealed with electrical tape and parafilm, and stored inside of the glovebox. $AlBr_3$ crystals (26.6 mg, 266.694 g/mol, 0.10 mmol) were dissolved in toluene (2 mL, 1.7 g) in a vial, and likewise sealed and stored inside of the box (stable for up to ~2 weeks). The $Al(O^sBu)_3$ solution was prepared by diluting with toluene to obtain a 50 mM concentration like the $GaCl_3$ and $AlBr_3$ solutions. Similarly, BBr_3 solution was diluted with pentane to obtain a 50 mM concentration. Before opening the bottles of Lewis acids, the glovebox was purged for > 20 minutes to minimize concentration of O_2 and H_2O in the atmosphere.

4.2.3 *Lewis acid suspensions*

$B(C_6F_5)_3$ powder (25.6 mg, 0.05 mmol) was suspended in toluene (5 mL, 4.3 g). Since $B(C_6F_5)_3$ is sparingly soluble in toluene, most of the powder stayed undissolved. The resulting suspension was mixed for 1 hour, then sealed and stored inside of the box until further use. Similarly, saturated solutions and suspensions of $AlCl_3$ powder, $Al(O_2CC_{17}H_{35})_3$, and BPh_3 were prepared.

4.3 Treatment of *exf*-BP with Lewis acids

1-2 mL of the desired Lewis acid stock solution or suspension was passed through a glass filter (~1 cm in diameter, fitted to a Pasteur pipette) to remove any impurities or undissolved solids.

The filtrate was used to completely submerge a black phosphorus sample freshly exfoliated onto a silicon substrate. After 1 hour, the substrate was washed with toluene (5x, 1.5 mL), allowed to soak in toluene for 10 min, then washed again with toluene (5x, 1.5 mL), then finally washed with pentane (5x, 1.5 mL) to remove traces of toluene.

4.4 Ambient Stability Tests of Lewis acid-treated *exf*-BP

Ambient stability tests were performed by securing the substrate on a microscope slide, and lightly capping it with a plastic petri dish cover, such that air and moisture can flow, but minimizes dust build-up. The laboratory lights were kept on for the duration of the measurements for consistency. Images (OM or AFM) were taken at indicated time points, over several days.

4.5 Fabrication and Testing of $AlBr_3$-treated *exf*-BP FET

The electrodes were patterned onto a standard thermal oxide wafer (300-nm-silicon-oxide layer on p-type silicon wafer) by standard photolithography (AZ1512 photoresist and Heidelberg Direct Write Lithography 66+), according to the structure shown in Figure 2.12, followed by metal deposition (5-nm-Ti/50-nm-Au with Electron beam evaporator) and lift-off.

In a glovebox equipped with an optical microscope transfer set-up, bulk black phosphorus was cleaved by micromechanical exfoliation onto a PDMS stamp. Thinner and larger flakes of black phosphorus were searched from the microscope by the contrast and color of the flake. The size of the flake was chosen to have enough area to cover the pre-patterned electrodes with 6-um separation. The position of the target flake is identified and aligned on the pre-patterned electrode. After making contact of the substrate and PDMS stamp with BP flake, the flake was transferred onto the patterned electrode. The flake was then treated with $AlBr_3$ solution according to the procedure in Section 4.3 (p. 32).

The photocurrent measurements were performed by scanning both gate and source/drain (S/D) biases at a fixed laser wavelength (1550 nm), and by measuring S/D currents. Two Keithley 2400 series source measure units (SMUs) were utilized in the measurements, one to apply the gate bias, the other to apply the S/D bias and record the current readings. The gate modulation and *I*–*V* measurement can be taken from the same measurement set up without the laser on, or the dark current measurement.

Section 5: References

(1) Pauling, L.; Simonetta, M. Bond Orbitals and Bond Energy in Elementary Phosphorus. *The Journal of Chemical Physics* **1952**, *20* (1), 29–34. https://doi.org/10.1063/1.1700191.

(2) Bridgman, P. W. FURTHER NOTE ON BLACK PHOSPHORUS. *J. Am. Chem. Soc.* **1916**, *38* (3), 609–612. https://doi.org/10.1021/ja02260a008.

(3) Hultgren, R.; Gingrich, N. S.; Warren, B. E. The Atomic Distribution in Red and Black Phosphorus and the Crystal Structure of Black Phosphorus. *The Journal of Chemical Physics* **1935**, *3* (6), 351–355. https://doi.org/10.1063/1.1749671.

(4) Brown, A.; Rundqvist, S. Refinement of the Crystal Structure of Black Phosphorus. *Acta Crystallographica* **1965**, *19* (4), 684–685. https://doi.org/10.1107/S0365110X65004140.

(5) Tofan, D. *Black Phosphorus*.

(6) Bridgman, P. W. Two New Modifications of Phosphorus. *Journal of the American Chemical Society* **1914**, *36* (7), 1344–1363. https://doi.org/10.1021/ja02184a002.

(7) Köpf, M.; Eckstein, N.; Pfister, D.; Grotz, C.; Krüger, I.; Greiwe, M.; Hansen, T.; Kohlmann, H.; Nilges, T. Access and in Situ Growth of Phosphorene-Precursor Black Phosphorus. *Journal of Crystal Growth* **2014**, *405*, 6–10. https://doi.org/10.1016/j.jcrysgro.2014.07.029.

(8) Liu, H.; Neal, A. T.; Zhu, Z.; Luo, Z.; Xu, X.; Tománek, D.; Ye, P. D. Phosphorene: An Unexplored 2D Semiconductor with a High Hole Mobility. *ACS Nano* **2014**, *8* (4), 4033–4041. https://doi.org/10.1021/nn501226z.

(9) Novoselov, K. S. Electric Field Effect in Atomically Thin Carbon Films. *Science* **2004**, *306* (5696), 666–669. https://doi.org/10.1126/science.1102896.

(10) Novoselov, K. S.; Jiang, D.; Schedin, F.; Booth, T. J.; Khotkevich, V. V.; Morozov, S. V.; Geim, A. K. Two-Dimensional Atomic Crystals. *Proceedings of the National Academy of Sciences of the United States of America* **2005**, *102* (30), 10451–10453. https://doi.org/10.1073/pnas.0502848102.

(11) Castellanos-Gomez, A.; Vicarelli, L.; Prada, E.; Island, J. O.; Narasimha-Acharya, K. L.; Blanter, S. I.; Groenendijk, D. J.; Buscema, M.; Steele, G. A.; Alvarez, J. V.; et al. Isolation and Characterization of Few-Layer Black Phosphorus. *2D Materials* **2014**, *1* (2). https://doi.org/10.1088/2053-1583/1/2/025001.

(12) Peng, R.; Khaliji, K.; Youngblood, N.; Grassi, R.; Low, T.; Li, M. Midinfrared Electro-Optic Modulation in Few-Layer Black Phosphorus. *Nano Letters* **2017**, *17* (10), 6315–6320. https://doi.org/10.1021/acs.nanolett.7b03050.

(13) Li, L.; Yu, Y.; Ye, G. J.; Ge, Q.; Ou, X.; Wu, H.; Feng, D.; Chen, X. H.; Zhang, Y. Black Phosphorus Field-Effect Transistors. *Nature Nanotech* **2014**, *9* (5), 372–377. https://doi.org/10.1038/nnano.2014.35.

(14) Mao, N.; Tang, J.; Xie, L.; Wu, J.; Han, B.; Lin, J.; Deng, S.; Ji, W.; Xu, H.; Liu, K.; et al. Optical Anisotropy of Black Phosphorus in the Visible Regime. *Journal of the American Chemical Society* **2016**, *138* (1), 300–305. https://doi.org/10.1021/jacs.5b10685.

(15) Walz, K. *Structure of Bilayer BP Showing Inter- and in-Plane Interactions*.

(16) Walz, K. *Layer-Dependent Bandgap of BP Compared to Other 2D Materials*.

(17) Castellanos-Gomez, A. Black Phosphorus: Narrow Gap, Wide Applications. *J. Phys. Chem. Lett.* **2015**, *6* (21), 4280–4291. https://doi.org/10.1021/acs.jpclett.5b01686.

(18) Favron, A.; Gaufrès, E.; Fossard, F.; Phaneuf-Laheureux, A. L.; Tang, N. Y. W.; Lévesque, P. L.; Loiseau, A.; Leonelli, R.; Francoeur, S.; Martel, R. Photooxidation and Quantum Confinement Effects in Exfoliated Black Phosphorus. *Nature Materials* **2015**, *14* (8), 826–832. https://doi.org/10.1038/nmat4299.
(19) Abate, Y.; Akinwande, D.; Gamage, S.; Wang, H.; Snure, M.; Poudel, N.; Cronin, S. B. Recent Progress on Stability and Passivation of Black Phosphorus. **2018**, *1704749* (111), 1–13. https://doi.org/10.1002/adma.201704749.
(20) Ryder, C. R.; Wood, J. D.; Wells, S. A.; Yang, Y.; Jariwala, D.; Marks, T. J.; Schatz, G. C.; Hersam, M. C. Covalent Functionalization and Passivation of Exfoliated Black Phosphorus via Aryl Diazonium Chemistry. *Nature Chemistry* **2016**, *8* (6), 597–602. https://doi.org/10.1038/nchem.2505.
(21) Van Druenen, M.; Davitt, F.; Collins, T.; Glynn, C.; O'Dwyer, C.; Holmes, J. D.; Collins, G. Covalent Functionalization of Few-Layer Black Phosphorus Using Iodonium Salts and Comparison to Diazonium Modified Black Phosphorus. *Chemistry of Materials* **2018**. https://doi.org/10.1021/acs.chemmater.8b01306.
(22) Liu, Y.; Gao, P.; Zhang, T.; Zhu, X.; Zhang, M.; Chen, M.; Du, P.; Wang, G.-W.; Ji, H.; Yang, J.; et al. Azide Passivation of Black Phosphorus Nanosheets: Covalent Functionalization Affords Ambient Stability Enhancement. *Angew. Chem. Int. Ed.* **2019**, *58* (5), 1479–1483. https://doi.org/10.1002/anie.201813218.
(23) Zhao, Y.; Wang, H.; Huang, H.; Xiao, Q.; Xu, Y.; Guo, Z.; Xie, H.; Shao, J.; Sun, Z.; Han, W.; et al. Surface Coordination of Black Phosphorus for Robust Air and Water Stability. *Angewandte Chemie - International Edition* **2016**, *55* (16), 5003–5007. https://doi.org/10.1002/anie.201512038.
(24) Abellán, G.; Lloret, V.; Mundloch, U.; Marcia, M.; Neiss, C.; Görling, A.; Varela, M.; Hauke, F.; Hirsch, A. Noncovalent Functionalization of Black Phosphorus. *Angew. Chem. Int. Ed.* **2016**, *55* (47), 14557–14562. https://doi.org/10.1002/anie.201604784.
(25) Gusmão, R.; Sofer, Z.; Pumera, M. Functional Protection of Exfoliated Black Phosphorus by Noncovalent Modification with Anthraquinone. *ACS Nano* **2018**, *12* (6). https://doi.org/10.1021/acsnano.8b01474.
(26) Abellán, G.; Wild, S.; Lloret, V.; Scheuschner, N.; Gillen, R.; Mundloch, U.; Maultzsch, J.; Varela, M.; Hauke, F.; Hirsch, A. Fundamental Insights into the Degradation and Stabilization of Thin Layer Black Phosphorus. *J. Am. Chem. Soc.* **2017**, *139* (30), 10432–10440. https://doi.org/10.1021/jacs.7b04971.
(27) Wood, J. D.; Wells, S. A.; Jariwala, D.; Chen, K. S.; Cho, E.; Sangwan, V. K.; Liu, X.; Lauhon, L. J.; Marks, T. J.; Hersam, M. C. Effective Passivation of Exfoliated Black Phosphorus Transistors against Ambient Degradation. *Nano Letters* **2014**, *14* (12), 6964–6970. https://doi.org/10.1021/nl5032293.
(28) Doganov, R. A.; O'Farrell, E. C. T.; Koenig, S. P.; Yeo, Y.; Ziletti, A.; Carvalho, A.; Campbell, D. K.; Coker, D. F.; Watanabe, K.; Taniguchi, T.; et al. Transport Properties of Pristine Few-Layer Black Phosphorus by van Der Waals Passivation in an Inert Atmosphere. *Nat Commun* **2015**, *6* (1), 6647. https://doi.org/10.1038/ncomms7647.
(29) Jensen, W. B. The Lewis Acid-Base Definitions: A Status Report. *Chem. Rev.* **1978**, *78* (1), 1–22. https://doi.org/10.1021/cr60311a002.
(30) Gille, A. L.; Gilbert, T. M. Donor-Acceptor Dissociation Energies of Group 13-15 Donor-Acceptor Complexes Containing Fluorinated Substituents: Approximate Lewis Acidities of

(F3C)3M vs (F5C6)3M and the Effects of Phosphine Steric Bulk. *Journal of Chemical Theory and Computation* **2008**, *4* (10), 1681–1689. https://doi.org/10.1021/ct8001859.
(31) Timoshkin, A. Y.; Frenking, G. Gas-Phase Lewis Acidity of Perfluoroaryl Derivatives of Group 13 Elements. *Organometallics* **2008**, *27* (3), 371–380. https://doi.org/10.1021/om700798t.
(32) Bing, D.; Wang, Y.; Bai, J.; Du, R.; Wu, G.; Liu, L. Optical Contrast for Identifying the Thickness of Two-Dimensional Materials. *Optics Communications* **2018**, *406*, 128–138. https://doi.org/10.1016/J.OPTCOM.2017.06.012.
(33) Li, L.; Kim, J.; Jin, C.; Ye, G. J.; Qiu, D. Y.; Da Jornada, F. H.; Shi, Z.; Chen, L.; Zhang, Z.; Yang, F.; et al. Direct Observation of the Layer-Dependent Electronic Structure in Phosphorene. *Nature Nanotechnology* **2017**, *12* (1), 21–25. https://doi.org/10.1038/nnano.2016.171.
(34) Youngblood, N.; Chen, C.; Koester, S. J.; Li, M. Waveguide-Integrated Black Phosphorus Photodetector with High Responsivity and Low Dark Current. *Nature Photonics* **2015**, *9*, 247–252. https://doi.org/10.1038/NPHOTON.2015.23.
(35) Chen, C.; Youngblood, N.; Peng, R.; Yoo, D.; Mohr, D. A.; Johnson, T. W.; Oh, S. H.; Li, M. Three-Dimensional Integration of Black Phosphorus Photodetector with Silicon Photonics and Nanoplasmonics. *Nano Letters* **2017**, *17* (2), 985–991. https://doi.org/10.1021/acs.nanolett.6b04332.
(36) Hong, T.; Chamlagain, B.; Lin, W.; Chuang, H.-J.; Pan, M.; Zhou, Z.; Xu, Y.-Q. Polarized Photocurrent Response in Black Phosphorus Field-Effect Transistors. *Nanoscale* **2014**, *6* (15), 8978–8983. https://doi.org/10.1039/C4NR02164A.
(37) Low, T.; Engel, M.; Steiner, M.; Avouris, P. Origin of Photoresponse in Black Phosphorus Phototransistors. *Phys. Rev. B* **2014**, *90* (8), 081408. https://doi.org/10.1103/PhysRevB.90.081408.
(38) He, D.; Wang, Y.; Huang, Y.; Shi, Y.; Wang, X.; Duan, X. High-Performance Black Phosphorus Field-Effect Transistors with Long-Term Air Stability. *Nano Lett.* **2019**, *19* (1), 331–337. https://doi.org/10.1021/acs.nanolett.8b03940.

APPENDIX

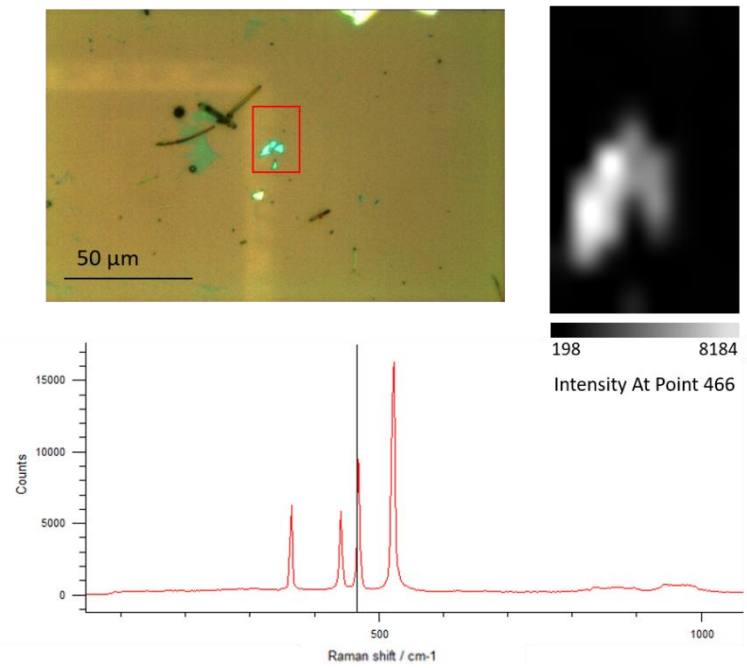

Figure A1. Raman microscope spectra (bottom), image (top left), and intensity mapping (top right) of $AlBr_3$-treated *exf*-BP.

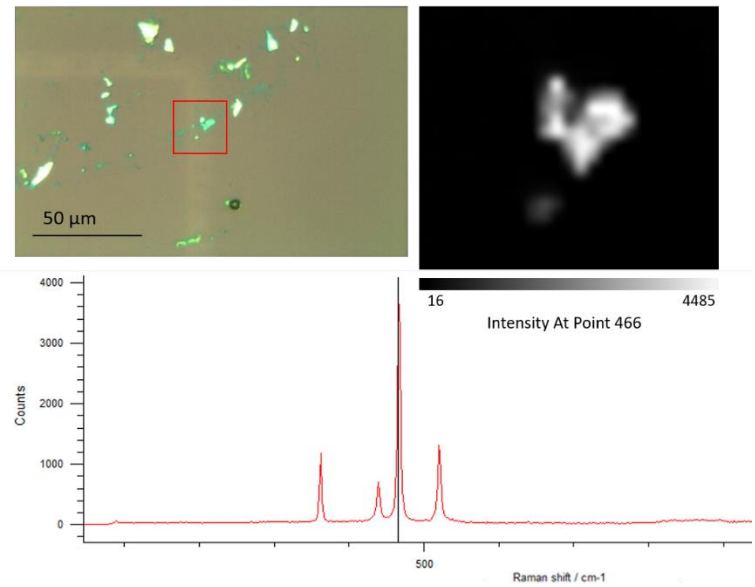

Figure A2. Raman microscope spectra (bottom), image (top left), and intensity mapping (top right) of BPh_3-treated *exf*-BP.

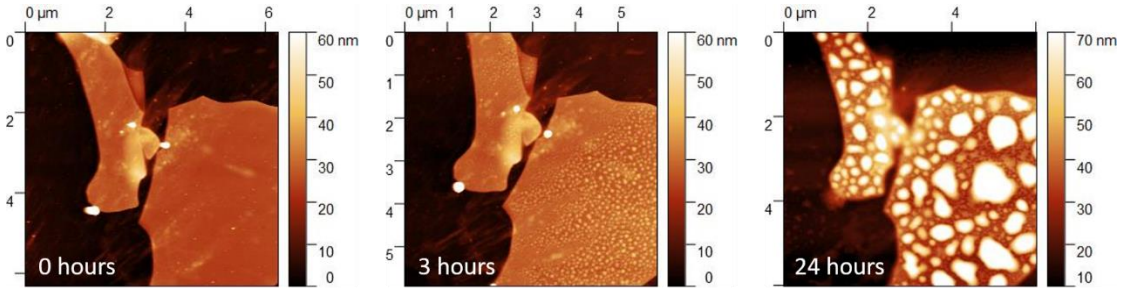

Figure A3. AFM ambient stability test of $Al(O^sBu)_3$-treated *exf*-BP.

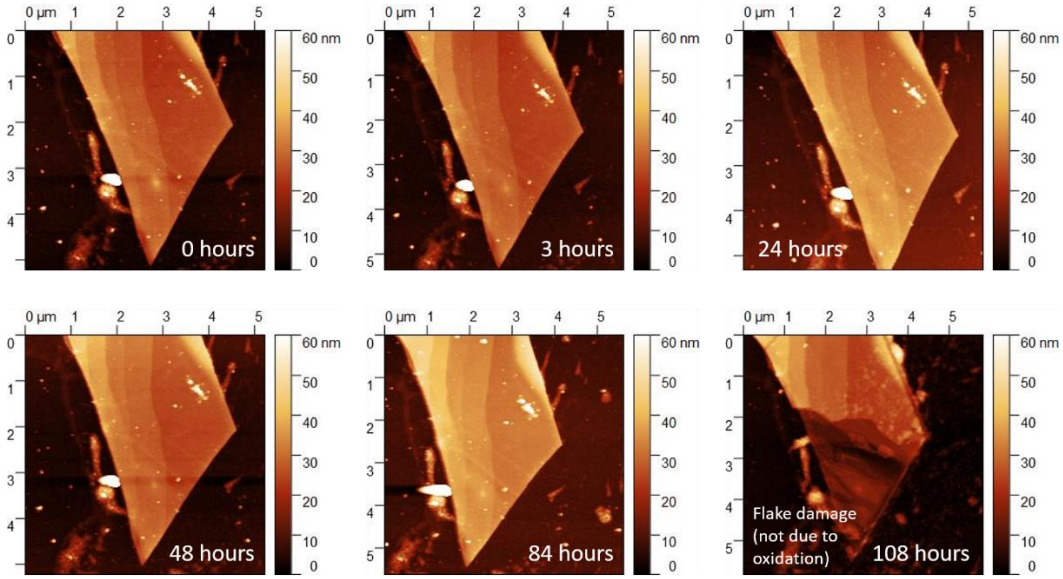

Figure A4. AFM ambient stability test of $AlBr_3$-treated *exf*-BP, continuing up to 4 days.